Polymer Vol. 39 No. 24 pp. 5913–5921, 1998
0032-3861/98/$ – see front matter
© 1998 Elsevier Science Ltd. All rights reserved
PII: S0032-3861(98)00121-9

Scanning force microscopy of polyester films: contact *versus* non-contact imaging and tip-induced wear experiments

John S. G. Ling[a], Graham J. Leggett[a,*] and Andrew J. Murray[b]
[a]*Department of Materials Engineering and Materials Design, The University of Nottingham, University Park, Nottingham NG7 2RD, UK*
[b]*TopoMetrix Corporation, 18 Hill Street, Saffron Walden, Essex CB10 1JD, UK*
(Received 16 December 1997; accepted 22 January 1998)

Two types of biaxially oriented poly(ethylene terephthalate) film have been examined using scanning force microscopy (SFM). For Mylar D, a material containing silicate surface additives, non-contact-mode and single-scan contact-mode SFM were found to yield essentially similar topographical data. At elevated loads, contact-mode SFM results in the direct modification of sample topography. Ridged structures were observed to form following repeated scanning of both materials at increased contact force. Generally, damage was significant at loads > 10 nN; however, repeat scanning (five times) was found to cause wear at loads as small as 2 nN. Lateral force microscopy revealed that the debris which accumulated along the perimeter of the worn region exhibited a high frictional response. We speculate that this debris results from the displacement of low-molecular-weight material or polymer chain fragments. Tip-induced wear under liquid led to the formation of worn regions with a smooth morphology. The wear mechanisms in operation during contact-mode SFM at loads greater than 10 nN probably include both mechanical deformation and adhesion components. © 1998 Elsevier Science Ltd. All rights reserved.

(Keywords: scanning force microscopy; wear; poly(ethylene terephthalate)

INTRODUCTION

Many of the interfacial interactions of polymeric materials are influenced by their surface chemistry and topography. While the past two decades have seen dramatic advances in our ability to characterize polymer surface chemistry by spectroscopic techniques (including, most notably, X-ray photoelectron spectroscopy and secondary ion mass spectrometry), attempts to characterize the topographies of polymer films by electron microscopy have been confronted by serious experimental difficulties. In particular, polymers degrade rapidly under electron bombardment, and are subject to rapid charging, leading to a requirement for the implimentation of pre-preparation procedures which are typically complex. Therefore, while electron microscopy has provided valuable data on the structures of bulk polymeric materials, scanning electron microscopy (SEM) has failed to provide the information necessary to develop an adequate understanding of the influence of polymer surface morphology on interfacial phenomena. The advent of scanning force microscopy (SFM) promises to facilitate the development of a much deeper understanding of polymer surface structure–property relationships, and recent years have seen a rapid growth of activity across a broad front, encompassing polymer crystals[1–4], films[5–10] and Langmuir–Blodgett monolayers[11].

While it is clear that SFM yields topographical data directly and with superior resolution to SEM, it is perhaps in the characterization of local properties that SFM-based techniques offer the most promise. Recent years have seen elegant empirical studies of force interactions between functionalized SFM tips and flat surfaces. Ducker *et al.*[12] have measured the force between a single colloidal sphere, attached to an SFM tip, and a planar silica surface. Lee *et al.* have functionalized spherical silica probes with biotinylated bovine serum albumin[13] and DNA oligomers[14], and measured the strengths of their interactions with, respectively, streptavidin and surfaces functionalized with DNA oligomers. Besides force–distance measurement, other techniques have been developed which are promising means by which local polymer surface properties may be investigated. In lateral force microscopy (LFM), frictional forces in the plane of the surface may be measured, enabling the spatial distribution of chemistries with differing surface energies to be mapped[15]. In a different application, Nisman *et al.*[3] have observed anisotropic local friction at the surface of a polymer single crystal using LFM, an effect attributed to changes in directionality of the chain folds in the fold plane of the crystal. In many engineering applications, local mechanical properties are important. Force modulation microscopy (FMM) utilizes an oscillating probe in contact with the sample surface to map local mechanical responses[16]. In certain circumstances, the contrast in FMM may reflect the local stiffness of the sample; in other circumstances, however, the origin of the contrast observed in FMM is more complex[17].

Many of the SFM techniques utilized to probe the surface properties of materials are contact-mode methods, including LFM, which offers great potential for mapping the frictional and adhesive properties of polymer surfaces. However, because polymers are easily deformed mechanically, the question of sample damage is a critical one. Any plastic

* To whom correspondence should be addressed: Department of Chemistry, UMIST, PO Box 88, Manchester, M60 IQD

deformation of the sample surface during imaging would present interpretational difficulties. It is therefore necessary to establish whether it is possible to operate in contact mode without causing sample damage, and to determine the mechanism of plastic deformation of the surface in regimes where damage does occur. In the present study, we have attempted to address these problems for two types of commercially produced poly(ethylene terephthalate) (PET) film: Du Pont Mylar D and ICI Melinex O ('Mylar' is a trade mark of the Du Pont company and 'Melinex' is a trade mark of ICI plc). Mylar D contains particulate additives at its surface, and has previously been extensively characterized by SFM[17], while Melinex O is free of additives.

The disruption of polymer surfaces during imaging in contact mode has been reported by other workers[18–22]. However, the dependence of the resulting morphology on the nature of the polymer and its properties (e.g. crystallinity, orientation, the presence or otherwise of additives, etc.) has not been investigated systematically. The formation of rippled or ridged structures has been reported by Leung and Goh[22] in studies of amorphous polystyrene. In contrast, the PET films used here are highly crystalline (*ca*. 50%) and exhibit biaxial orientation induced by drawing in orthogonal directions to elongations of *ca*. $\times 3.5$. We have compared the behaviour observed for semicrystalline PET with that reported for amorphous polystyrene (PS), and have examined the influence of film orientation on tip-induced sample deformation. Wawkuschewski *et al*.[20] have reported periodic contrast variations in contact-mode images of oriented polyethylene tape samples, and have reported the formation of oriented rippled structures following repeated imaging at raised forces. An important objective was to examine whether similar effects would be observed as a consequence of SFM tip interactions with PET films of known orientation.

EXPERIMENTAL

Samples of Mylar D were obtained from Goodfellow Advanced Materials (Cambridge, UK) and were used as received. Mylar D is a commercial biaxially oriented PET film produced by Du Pont. Samples of biaxially oriented O grade Melinex (ICI, Wilton, UK) were supplied with two clean sides facing and were used as received. The materials were characterized using surface analytical techniques (X-ray photoelectron spectroscopy and static secondary ion mass spectroscopy) and were found to be free of adventitious contamination, yielding spectra (not shown) in agreement with those widely reported in the literature.

SFM was performed in contact mode using a TopoMetrix Explorer scanning probe microscope (TopoMetrix Corporation, Saffron Walden, UK). Images were recorded under ambient conditions (except where noted otherwise) using commercially fabricated pyramidal silicon nitride tips (TopoMetrix Corporation) with radii of 50 nm, attached to 2- or 150-μm heads and having nominal force constants of either 0.032 or 0.064 N m^{-1}. It is important to note that these force constants may be subject to errors of $\pm$ 50%, leading to an inherent uncertainty in the precise force used during contact-mode imaging. However, for a given tip, the imaging force may be controlled by altering the position of the deflected laser beam on the photodetector *via* adjustment of a 'set point'. As constant-force-mode imaging was used, the maximum laser deflection also represented the maximum permissible imaging force. Hence, manipulation of the set point during feedback gave rise to a range of relative imaging forces. These relative forces could be converted into absolute forces after performing a force–distance measurement given knowledge of the cantilever force constant and the detector signal immediately prior to the tip making contact with the sample. Therefore, although there is inherent uncertainty in the absolute force used, the distinction between 'low' and 'high' force imaging could be rigorously maintained for a given cantilever, and a controlled proportionality between the two regimes of operation could be established. Typical imaging forces were in the range 1–5 nN in 'low force' mode; however, during tip-induced wear experiments, higher forces were used (in the range 10–45 nN). These ranges of force take account of the uncertainty arising from the uncertainty in the cantilever spring constant; the two regimes are therefore quantitatively distinct in terms of the magnitudes of the forces used.

'Non-contact' mode enables imaging with a minimal lateral force (although occasional tip–surface contacts may occur). Amplitude detection mode was employed, in which silicon cantilevers (nominal spring constant 50 N m^{-1} and tip radii 20 nm) were resonated at 150 kHz, with feedback achieved at 50% of the free air resonance amplitude. The feedback loop maintains the probe at constant oscillation amplitude during imaging.

RESULTS

Comparison of contact and non-contact imaging of Mylar D

Mylar D is treated during manufacturing to incorporate

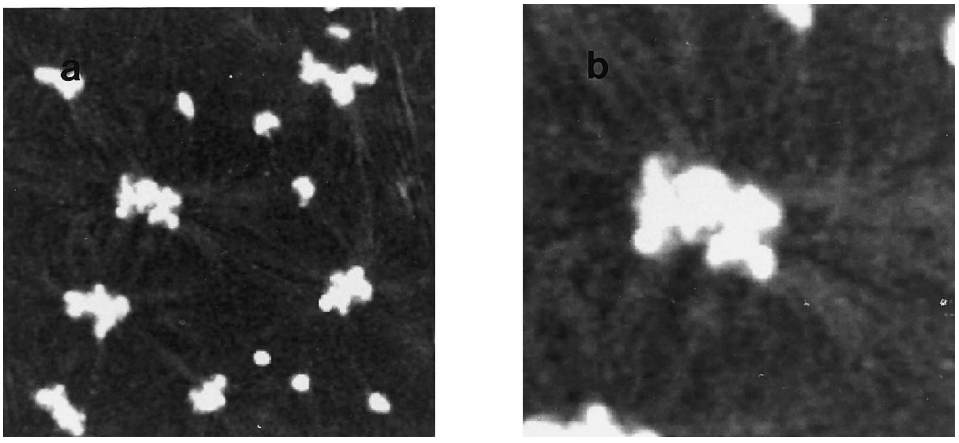

Figure 1 Contact-mode SFM images of Mylar D. Image sizes: (a) 3 μm $\times$ 3 μm; (b) 1.34 μm $\times$ 1.34 μm

silicate additive particles at the film surface. These additive particles may be seen in SEM images, and were observed in contact-mode SFM topographical images (*Figure 1*). The silicate additives were observed as globular features, with diameters at the surface in the range 100–500 nm, which typically protrude some 20–40 nm above the film surface. The particle diameters were found to agree closely with those determined by SEM. Some of the larger particles appeared to be clusters of smaller particles (*Figure 1a*). Radiating structures were observed (*Figure 1b*) around some of these larger inclusions. These features were raised 1–4 nm above the surrounding polymer surface, they typically exhibited widths in the range 70–110 nm (not corrected for any tip-induced broadening effects) and they formed shallow ridges up to 500 nm in length.

The appearance of the silicate particles in the non-contact-mode images (*Figure 2*) was very similar to that exhibited in the contact-mode images. Furthermore, typical dimensions measured using non-contact mode were similar to those measured using contact mode. The radial features may be observed in *Figure 2a*, and they are very similar in their morphology to the features observed in *Figure 1b*.

Tip-induced wear of Mylar D

Contact-mode imaging yielded similar topographical characteristics for Mylar D surfaces to those observed in non-contact mode, *provided the imaging force was minimized and provided the sample was not scanned repeatedly*. Increasing the imaging force above the minimum required to record a stable, well-resolved image led to modification of the sample surface, while repeat scanning (five times) was, on occasions, observed to cause sample damage at loads as small as 2 nN. *Figure 3* shows a region of a Mylar D sample which has been imaged at minimal force in contact mode following imaging of the central region, enclosed by a box in *Figure 3a* and shown in expanded form in *Figure 3b*, at elevated force. A rippled morphology has formed, with the ripples running approximately vertically across the region imaged at elevated force, and exhibiting widths in the range 70–130 nm. The development of surface morphology during repeat scanning is illustrated in *Figure 4*, which shows the development of a cross-section through a single particle with increasing numbers of scans at a contact force of 10 nN. The development of topographical features is clearly seen. The position of the silicate particle remains unperturbed by the process of repeated imaging, however, indicating that it is firmly embedded in the polymeric matrix.

Tip-induced wear of Melinex O

Modifications of the Mylar D surface at low contact forces could be influenced by the presence of the additive particles. Therefore, to specifically study the development of wear-induced morphology in the polymer itself, we

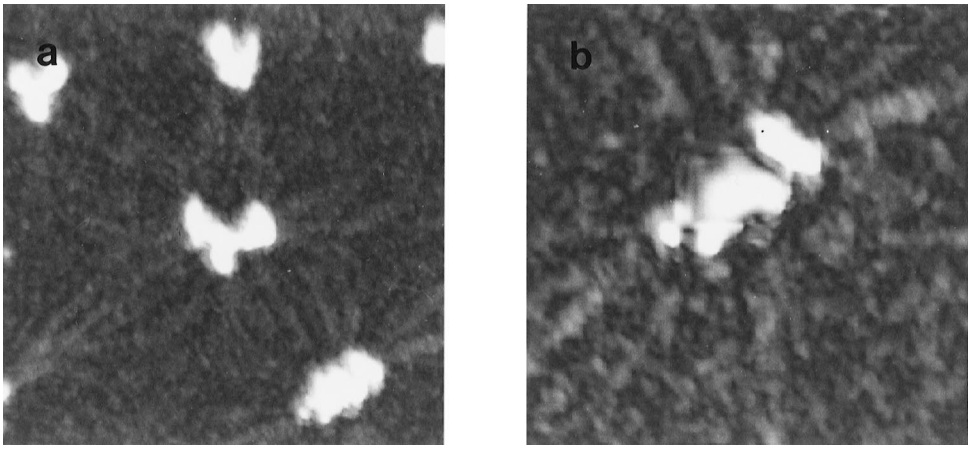

Figure 2 Non-contact-mode SFM images of Mylar D. Image sizes: (a) 2 μm $\times$ 2 μm; (b) 1.1 μm $\times$ 1.1 μm

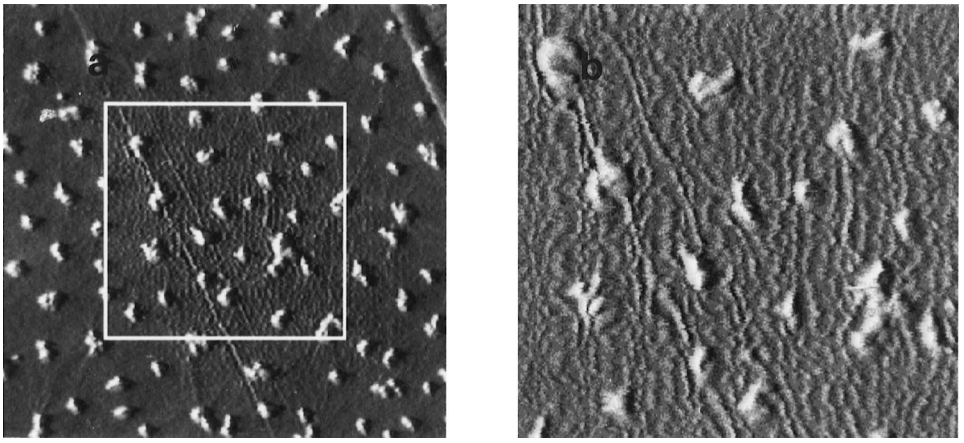

Figure 3 Effects of tip-induced wear at elevated force in contact mode. (a) A region of Mylar D imaged at low force following repeat scanning of the region in the box at elevated force. Image size: 7.5 μm $\times$ 7.5 μm. (b) Enlargement of the worn region in (a), showing the rippled morphology

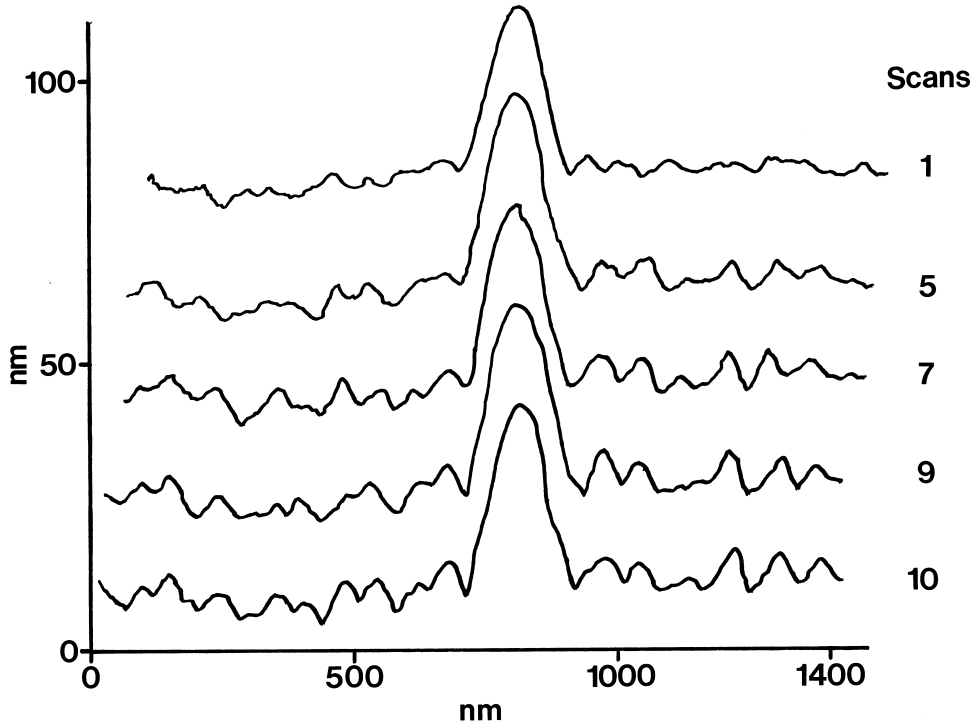

Figure 4 Development of the cross-section through a single silicate particle with repeated scanning at increased force in contact mode

examined a material which contained no additives: O grade Melinex. Melinex O exhibits a very smooth morphology (*Figure 5*) when imaged in contact mode with minimal force. The surface has the appearance of being composed of small hillocks superimposed on a gently rolling surface; however, the range of variation in the *z*-direction in *Figure 5* is only 20 nm over an area of 9 μm^2. There is no evidence that the morphology of the polymer is influenced by the imaging process under these conditions, and very similar images were recorded in non-contact mode.

Increasing the imaging force to 30 nN in contact mode produced a similar morphology to that observed for Mylar D: ridges were observed to form (*Figure 6*), running perpendicular to the scan direction, which was oriented horizontally. During scanning, the tip moves rapidly from left to right and back across the scanned region, with the image accumulating through slower incremental advances from top to bottom across the imaged region. The scan direction is defined as the direction of rapid movement of the tip. In *Figure 6*, the tip was scanned rapidly from left to right across the image, advancing slowly from the top of the image to the bottom as the image accumulated. After one scan (*Figure 6a*), little detail was evident; the resulting image was clearly of poorer quality than the image shown in *Figure 6*, but pronounced ridges were not yet evident. After three scans (*Figure 6b*), the ridge structures were more clearly evident. However, the orientation of the ridges with respect to the scan direction was, to some extent, variable: some of the ridges formed arcs (albeit with low curvatures) or forks, and not all were oriented at exactly 90° to the scan direction. After five scans (*Figure 6c*), these features exhibited heights in the range 8–27 nm and widths in the range 180–240 nm.

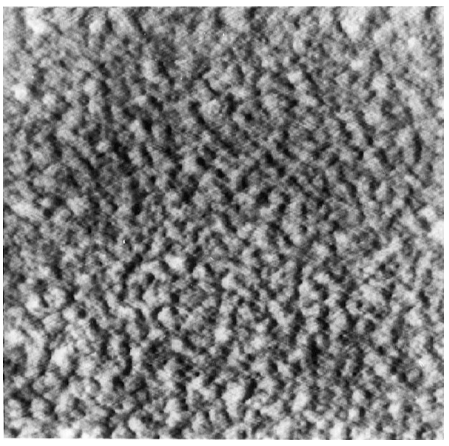

Figure 5 Contact-mode SFM image of a Melinex O surface. Image size: 3 $\mu m \times 3$ μm

Like Mylar D, Melinex O is a biaxially oriented material. It is manufactured by extruding molten polyester onto a cold drum. The polymer is drawn in the forward direction (the machine direction, MD) to several times its original elongation, following which it is drawn a second time in an orthogonal direction (the tranverse draw direction, TD). The drawing processes lead to molecular orientation and strain-induced crystallization in the film. In order to determine whether the orientation of the polymer molecules exerted an influence over the morphology developed at the surface during tip-induced wear, we performed experiments in which the scan direction of the SFM was aligned at a known orientation with respect to the forward draw or machine direction.

Figure 7a shows an image of a sample that has been scanned five times at elevated force with a scan direction of 90° with respect to the MD. The tip was then retracted and the sample rotated through 90° (the scan direction was then effectively oriented at 0° to the MD). The sample was then scanned five times at the same force (15 nN) to yield the image shown in *Figure 7b*. The experiment was repeated with a new tip and a new sample, but with the sequence of experiments reversed in each case. Similar images resulted.

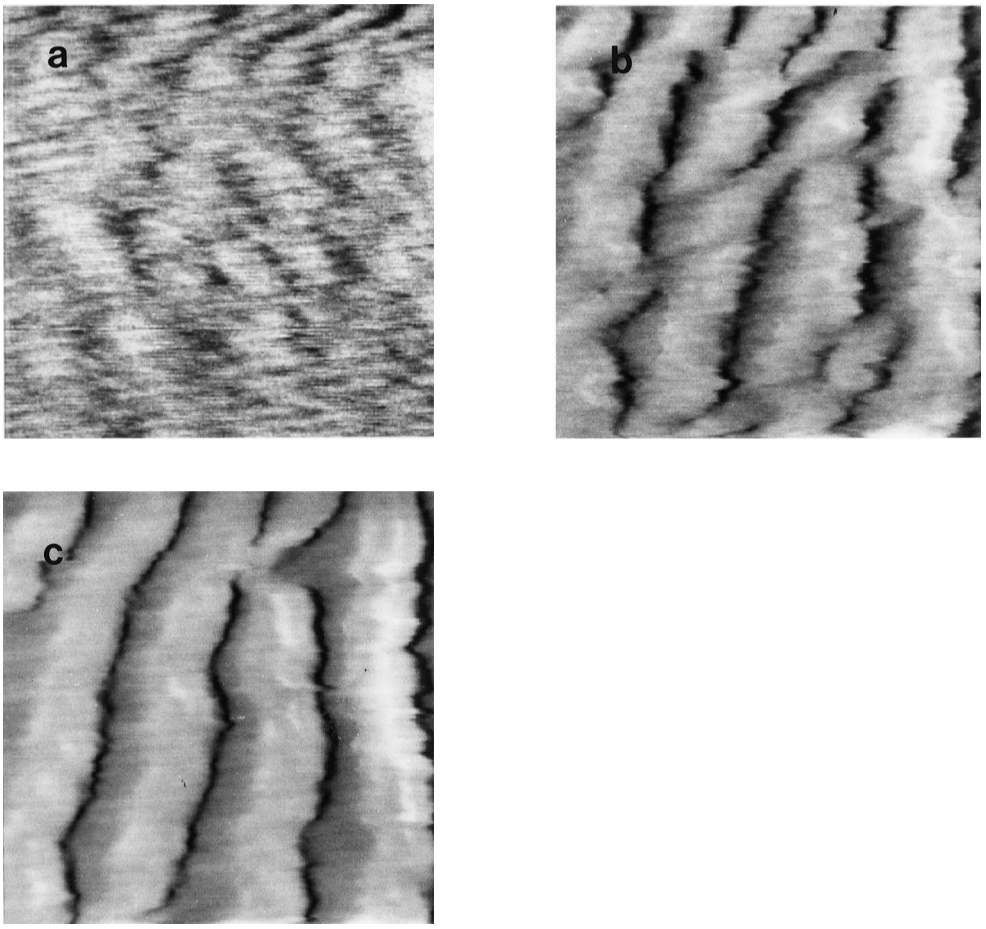

Figure 6 Development of surface topography in Melinex O with repeat scanning at elevated force in contact mode. (a) One scan; (b) three scans; (c) five scans. Image size: 894 nm × 894 nm (all images)

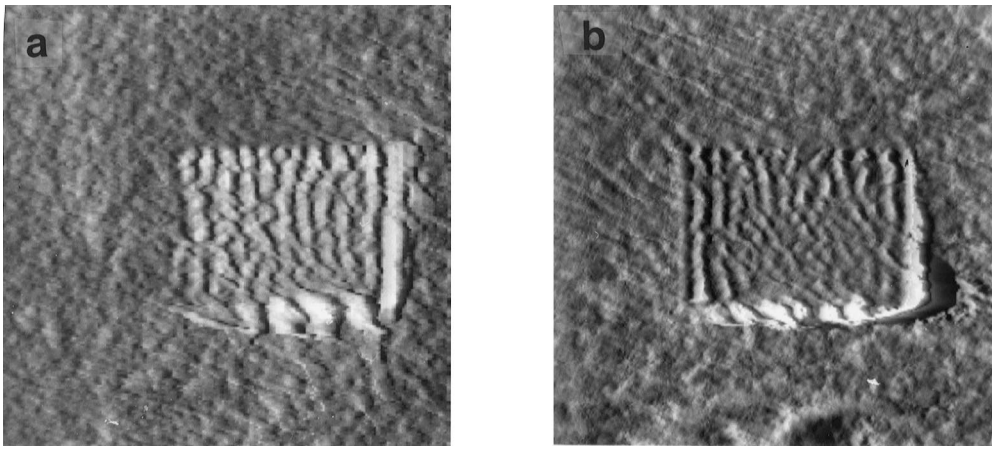

Figure 7 Low force topographical images of two separate regions of Melinex O following wear at increased load. Orientation of scan direction with respect to machine direction: (a) 90°; (b) 0°. Image size: 3 μm × 3 μm (both images)

In order to investigate the composition of the worn region further, LFM images were recorded. *Figure 8* shows LFM images of a region that has been worn during five scans at elevated force (15 nN), recorded in the forwards and the backwards directions. The debris which has accumulated along the bottom edge of the worn region shows up with dark contrast in the forwards direction LFM image, and with light contrast when the scan direction is reversed.

In air, there is a substantial adhesive interaction between the SFM tip and the sample surface, due to the capillary force between the tip and the water film that typically covers the sample surface. The thickness of the water film, and the magnitude of the capillary force, are influenced by ambient conditions; however, under the conditions prevailing in the authors' laboratory, the capillary force is typically in the range 20–30 nN. During sliding contact between the tip and the surface, this capillary force may lead to an additional adhesive contribution to the interaction force. In order to examine the possible effect of capillary forces on wear, experiments

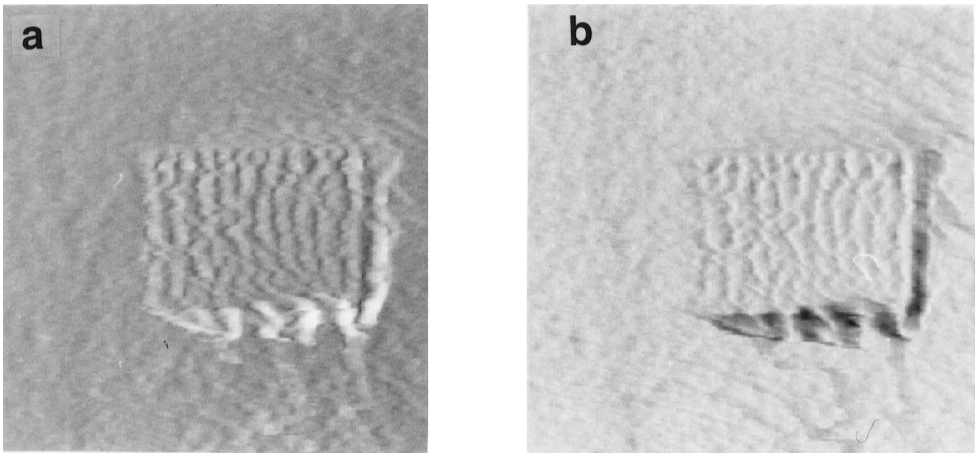

Figure 8 LFM images of the region shown in *Figure 9a* in the reverse direction (a) and the forwards direction (b). Image size: 3 μm $\times$ 3 μm (both images)

were performed using similar contact forces to those used to create wear in air, but under liquid. *Figure 9* shows topographical images of a region that has been subjected to five repeat scans at a force of 10 nN under water. The sample worn under liquid exhibits a morphology that is strikingly different from that observed in *Figures 7* and *8*. While a worn region may still be clearly seen, its surface is significantly smoother and the edges of the worn region are sharply defined. Moreover, there appears to be no accumulation of debris along any of the perimeters of the worn area. LFM images (*Figure 10*) do appear to indicate an enhanced frictional response along one edge in particular, giving rise to an inversion of contrast on reversal of the scan direction (the lower edge in *Figure 10*), but this region is narrow and sharply defined in comparison with the broad area in *Figure 8*, which appears to be composed of debris.

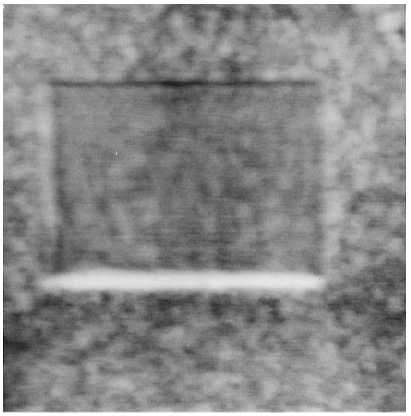

Figure 9 Contact-mode SFM images of a region of a Melinex O sample worn by repeated scanning under liquid. Image size: 2.3 μm $\times$ 2.3 μm

DISCUSSION

Comparison of contact and non-contact topographical images

Comparison of the topographical images in *Figures 1* and *2* reveals that there is little difference between the morphologies observed in contact and non-contact modes for these materials. In particular, the morphology of the polymeric material surrounding the silicate inclusions is revealed with clarity in both modes. Radial structures are observed to emanate from some of the larger silicate particles, and the observation of these features in non-contact mode supports our earlier suggestion[17] that these features are real features of the polymeric matrix in Mylar D. The origin of the radiating features is not clear; however, one possible explanation[17] is that they are the consequence

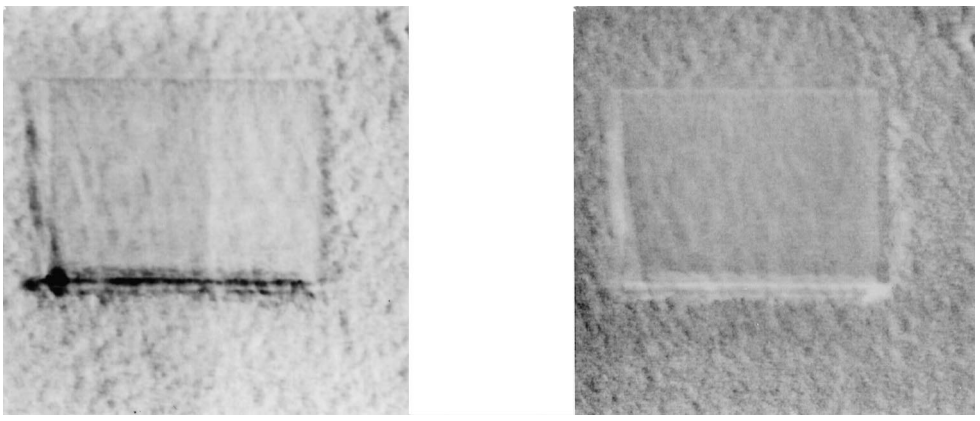

Figure 10 LFM images of a sample of Melinex O following wear at elevated force under liquid. (a) The forwards direction scan. (b) The reverse direction scan. Image size: 2.3 μm $\times$ 2.3 μm (both images)

of strain-induced crystallization around the additive particles. Local strain within the polymer film may be greater around the larger additive particles (the radiating structures are predominantly absent from images of smaller silicates).

The observation of an apparently unperturbed surface during contact-mode imaging of Melinex O indicates that the use of non-contact imaging is not essential if reliable topographical data are to be obtained, provided adequately low contact forces are employed and single scans are employed. We conclude, on the basis of the present data, that a contact force of less than 5 nN must be employed if images of an essentially undamaged surface are to be recorded. However, repeat scanning of the same region, even at loads as small as 2 nN, was observed to lead, ultimately, to the formation of ridged morphologies. Given this restriction of the experimental parameters, there is still considerable scope for the utilization of a number of contact-mode techniques that are designed to explore nanoscale surface properties (such as friction, probed by LFM), although some modified surfaces, such as those of plasma-treated polymers, may contain more delicate morphologies (composed of low-molecular-weight material) that are more easily disrupted[23].

Tip-induced wear

Studies of the effects of imaging with elevated force during contact mode are important because they enable a non-destructive regime of operation to be delineated, they can provide fundamental insights into the mechanical interactions that occur between the SFM tip and the sample, and they may provide insights into the nanoscale tribological interactions of polymeric materials, of significance to a number of fields of study.

Other workers have also examined tip-induced wear of polymer surfaces, and have described the formation of rippled or ridged structures as a result of tip-induced wear processes. Hamada and Kaneko[18,19] have deliberately created grooves in polymer surfaces in order to elucidate mechanisms of nanoscale wear, although the features that they created were on a much coarser scale than those reported above, and were created by loads which were two orders of magnitude greater than those employed in the present study. There have also been reports of the existence of oriented topographical features at the surfaces of oriented polymers. For example, Wawkuschewski *et al*.[20] reported periodic contrast variations in contact mode images of oriented polyethylene tape samples, and reported the formation of rippled structures following imaging at high contact forces. However, there have been few studies of the nanotribological properties of PET surfaces that have combined such small scale and such small loads as those employed in the present study. Bhushan and Koinkar[21] have previously performed studies with loads in the μN range.

The work of Leung and Goh[22], who reported the formation of a rippled morphology on PS surfaces imaged in contact mode, is of particular relevance to the present study. Their contact forces, of the order of 100 nN, were higher than ours, which were at most 45 nN, and their samples were also amorphous, whereas the PET films we have examined in the present study were significantly crystalline (*ca*. 50%). However, despite these differences, the phenomena observed are qualitatively very similar.

Both the PS studied by Leung and Goh and the PET employed in the present work have a glass transition temperature significantly above room temperature, although concepts relating to the bulk structure of the material may have limited validity when applied to the surface region. For example, Keddie *et al*.[24] have suggested that the glass transition temperature of the PS surface differs from that of the bulk polymer. They suggest that a liquid-like or viscous film exists at the surface of the glassy polymer. This surface phase may deform under tip-induced wear in a different fashion from that expected for an elastic, glassy surface layer. In particular, if the depression of T_g is of the order of a few tens of degrees (for example, they suggest that the depression is 35°C for an 8-nm-thick PS film[25]), then the surface phase may behave in a rubbery fashion and the Schallamach wave model[26], developed to describe the interaction between a hard slider and a rubber surface, may be applicable. However, we see little evidence of elastic recovery of the surface, so that whereas the Schallamach model describes the creation of wave structures which ultimately relax to yield the original surface morphology, the deformation in our situation must be plastic.

Meyers *et al*.[27] also studied PS wear with an SFM probe, using loads of the order of 15 nN (and therefore directly comparable with the loads used in our 'high force' experiments). They compared the wear-induced morphology of polymers with four different molecular weights (MWs). They observed oriented ridges in worn regions of samples with MW $>$ 100 000, similar in form to those which we have reported above. Meyers *et al*. reported a dependence of the wear-induced morphology on the polymer MW, with lower MW materials exhibiting a coarser morphology (described by the authors as an abrasion pattern). However, both morphologies exhibited orientation perpendicular to the scan direction. Meyers *et al*. interpreted their data in terms of a plastic analogue of the Schallamach wave[26], evolving under load *via* irreversible deformation. This process could involve pulling combined with stretching of entanglements at the PS surface. They speculated that adhesion during sliding of the SFM tip may lead to the partial disentanglement of molecules at the surface; when the shear force of the contacted tip exceeds the adhesive forces, the stretched macromolecule recoils.

Qualitatively, there is great similarity between the ridged structures formed during tip-induced wear of PET at high contact forces and the morphologies reported by Leung and Goh and Meyers *et al*. The data in *Figure 9* provide an important insight into the origin of these morphologies. Critically, the ridged morphology is not observed when the wear experiment is performed in an aqueous environment; while a depressed region is still observed where the sample has been scanned repeatedly, its surface is smooth. Thus, in both cases, the sample is deformed by the action of the tip as it scans the surface under an applied load, but additionally, in air, the deformed material adopts a ridged morphology. We attribute this to the effect of the capillary force during wear in air. This force is substantial in magnitude and adhesive, but is absent in the experiment performed under liquid, and its presence means that the local friction force is stronger in air than under liquid. Thus, two components are identified in the tip–surface interaction: a deformation component (related to the applied load) and an adhesion component (related to the tip–sample adhesion). The alternative explanation, that the water molecules lubricate the tip–sample interaction in the experiment under water, may be discounted because a water film exists at the surface of the polymer in air too.

The mechanisms of deformation arising from the two different components of the wear interaction are clearly

different. The deformation-only wear under liquid results in a smooth morphology and the minimal accumulation of debris around the perimeter of the worn region. In contrast, the adhesive component causes the formation of ridges in air, probably through a mechanism analogous to a slip-stick mechanism, in which adhesion between the tip and the surface results in the pulling of surface material as the tip traverses the surface. Once adhesive contact has been made, material is pulled by the tip until it reaches a critical size or extension, at which point the polymer material breaks free from the tip, the tip makes a fresh adhesive contact and the process is repeated. Significantly, substantial amounts of debris accumulate around the perimeters of the worn region during wear in air, forming disordered features quite different to the narrow, linear debris feature at the lower side of the worn region in *Figures* and *10*.

LFM contrast arises from the twisting motion of the cantilver during imaging. While frictional interactions between the tip and the sample give rise to contrast, topographical variations may also cause components of the load to be resolved in the plane of the sample surface. Thus, there may be a topographical contribution to the LFM contrast. However, comparison of LFM data recorded with opposing scan directions assists in the separation of topographical and frictional effects, because frictional effects should yield inverted contrast when the scan direction is reversed, while topographical contributions should retain the same sign[28]. Our LFM data show that the debris which accumulates along the bottom of the worn regions has a high frictional interaction with the SFM tip, undergoing a contrast reversal when the scan direction is reversed. This indicates that there is a significant lateral (frictional) interaction between the tip and the sample over this debris. The ridges which run across the worn regions also exhibit contrast in LFM mode, but the contrast is similar in the forwards and reverse scan directions, indicating that it is largely the result of topographical variations which lead to torsional motions of the cantilever as it scans the sample[17].

It is concluded that the debris piled at the bottom of the scanned region in *Figure 8* is likely to be different in composition from the rest of the worn region, while the ridges are simply the result of a restructuring of the polymeric material in the worn area, in accordance with the model described above. The surface of Melinex O is thought to be very clean, and no traces of adventitious contamination were observed using X-ray photoelectron spectroscopy or static secondary ion mass spectroscopy. While cyclic trimer species have been observed previously in static secondary ion mass spectra of PET surfaces, they have only been produced at Melinex O surfaces by chloroform extraction (the trimer is present in the bulk at low levels and may be brought to the surface by extraction in a Soxhlet thimble[29]) or by heat treatment[30]. It is unlikely that the debris observed here is composed of cyclic trimer, unless the trimer is present at significant concentrations just below the sampling depth (*ca.* 1 nm) of static secondary ion mass spectroscopy. While adventitious contamination from atmospheric exposure undoubtedly occurs, the volume of debris produced is too great to have arisen from the accumulation of material from this source. Therefore, it seems that the debris is composed of either low-molecular-weight polymeric material, or, most likely, polymer chain fragments produced by the mechanical rupture of bonds at the surface, possibly produced via a mechanism similar to that proposed by Meyers *et al*., and described above.

Both Mylar D and Melinex O are oriented during manufacturing by elongation by a factor of 3.5 in orthogonal directions. These draw processes, combined with a final heat setting process, lead to a material that is highly oriented in two directions and highly crystalline (*ca.* 50%). Furthermore, there have been indications that orientation at the film surface may be even more extensive than in the bulk, because of the greater freedom of movement of the molecules at the surface during drawing[31]. However, the data in *Figure 7* show that molecular orientation in the unworn polymer film has no influence on the orientation of the ridge structures formed during wear at high contact forces. This is in contrast to the results of Wawkuschewski *et al.*[20], who observed the formation of ridge structures parallel to the direction of orientation in studies of drawn polyethylene. However, they employed significantly higher draw ratios ($\lambda = 10–70$) and, under such conditions, the formation of more extensively oriented structures may be expected.

CONCLUSIONS

Single-scan topographical data recorded for biaxially oriented polyester films using low force contact-mode and non-contact-mode SFM were found to be very similar. In both modes, radial features were observed to emanate from some of the larger silicate particles in samples of Mylar D. In contact mode, the polymer surface morphology may be modified by increasing the force employed. Ridges were observed to form, yielding a morphology qualitatively very similar to that reported by other workers in studies of a quite different material, PS. The polymer orientation exerted no influence on the resulting morphology. The debris that accumulated at the bottom of the scanned region was found to yield high contrast in LFM images, suggesting that it differed in composition from the rest of the polymer surface. We suggest that this was either low-molecular-weight polymeric material or, most likely, polymer chain fragments produced by bond rupture during tip–sample interactions. Studies of wear under liquid revealed that ridged structures were not formed, although wear still occurred. It is proposed that tip-induced wear is caused by two effects: deformation, due to the applied load, which leads to the movement of low-molecular-weight material and/or the formation of easily moved polymer chain fragments; and adhesion, due, in air, to the presence of a capillary force between the tip and the sample. The ridged morphology that results from tip-induced wear in air is due to a combination of both effects, while under liquid, there is no adhesive capillary interaction and a smooth morphology results.

ACKNOWLEDGEMENTS

The authors are grateful to Dr P. H. Shipway (University of Nottingham) and Professor D. Briggs (ICI) for helpful and stimulating discussions, and to Professor Briggs for kindly supplying Melinex O with a known orientation. J.S.G.L. thanks the EPSRC for a Research Studentship.

REFERENCES

1. Stocker, W., Schumacher, M., Graff, S., Lang, J., Wittman, J. C., Lovinger, A. J. and Lotz, B., *Macromolecules*, 1994, **27**, 6948.

2. Smith, P. F., Nisman, R., Ng, C. and Vancso, G. J., *Polym. Bull.*, 1994, **33**, 459.
3. Nisman, R., Smith, P. and Vancso, G. J., *Langmuir*, 1994, **10**, 1667.
4. Miles, M. J., Jandt, K. D., McMaster, T. J. and Williamson, R. L., *Coll. Surf. A*, 1994, **87**, 235.
5. Huang, J. Y., Li, J. S., Juang, Y.-S. and Chen, S.-H., *Jpn. J. Appl. Phys.*, 1995, **34**, 3163.
6. Lin, F. and Meier, D. J., *Langmuir*, 1994, **10**, 1660.
7. Haugstad, G., Gladfelter, W. L., Weberg, E. B., Weberg, R. T. and Jones, R. R., *Langmuir*, 1995, **11**, 3473.
8. Tanaka, K., Yoon, J.-S., Takahara, A. and Kajiyama, T., *Macromolecules*, 1995, **28**, 934.
9. Kajiyama, T., Tanaka, K., Ohki, I., Ge, S.-R., Yoon, J. S. and Takahara, A., *Macromolecules*, 1994, **27**, 7932.
10. Kajiyama, T., Ohki, I., Ge, S.-R. and Takahara, A., *Proc. Jpn. Acad. Ser. B*, 1995, **71**, 75.
11. Radmacher, M., Tilmann, R. W. and Gaub, H. E., *Biophys. J.*, 1993, **64**, 735.
12. Ducker, W. A., Senden, T. J. and Pashley, R. M., *Langmuir*, 1992, **8**, 1831.
13. Lee, G. U., Kidwell, D. A. and Colton, R. J., *Langmuir*, 1994, **10**, 354.
14. Lee, G. U., Chrisey, L. A. and Colton, R. J., *Science*, 1994, **266**, 771.
15. Wilbur, J. L., Biebuyck, H. A., MacDonald, J. C. and Whitesides, G. M., *Langmuir*, 1995, **11**, 825.
16. Maivald, P., Butt, H. J., Gould, S. A. C., Prater, C. B., Drake, B., Gurley, J. A., Elings, V. B. and Hansma, P. K., *Nanotechnology*, 1991, **2**, 103.
17. Ling, J. S. G. and Leggett, G. J., *Polymer*, 1997, **38**, 2617.
18. Hamada, E. and Kaneko, R., *Ultramicroscopy*, 1992, **42–44**, 184.
19. Kaneko, R. and Hamada, E., *Wear*, 1993, **162–164**, 370.
20. Wawkuschewski, A., Cantow, H.-J. and Magonov, S. N., *Adv. Mater.*, 1994, **6**, 476.
21. Bhushan, B. and Koinkar, V. N., *Tribol. Trans.*, 1995, **38**, 119.
22. Leung, O. M. and Goh, M. C., *Science*, 1992, **255**, 64.
23. Beake, B. D., Ling, J. S. G. and Leggett, G. J., submitted to *J. Mater. Chem.*
24. Keddie, J. L., Jones, R. A. L. and Cory, R. A., *Europhys. Lett.*, 1994, **27**, 59.
25. Keddie, J. L. and Jones, R. A. L., *Israel J. Chem.*, 1995, **35**, 21.
26. Schallamach, A., *Wear*, 1971, **17**, 301.
27. Meyers, G. F., DeKoven, B. M. and Seitz, J. T., *Langmuir*, 1992, **8**, 2330.
28. Grafstrom, S., Neitzert, M., Hagen, T., Ackerman, J., Neumann, R., Probst, O. and Wortge, M., *Nanotechnology*, 1993, **4**, 143.
29. Briggs, D., *Surf. Interface Anal.*, 1986, **8**, 133.
30. Reichlmaier, S., Bryan, S. R. and Briggs, D., *J. Vac. Sci. Technol. A*, 1995, **13**, 1217.
31. Walls, D. J. and Coburn, J. C., *J. Polym. Sci. B*, 1992, **30**, 887.